Prevention of lithium deposition reaction in Li-ion batteries using a non-invasive approach, Part I: Separation of the negative electrode contributions

Karrick Mergo Mbeya, Christophe Forgez, Guy Friedrich, Nicolas Damay, Khadija El Kadri Benkara

Graphical Abstract

Prevention of lithium deposition reaction in Li-ion batteries using a non-invasive approach - Part I : Separation of the negative electrode contributions.

Karrick Mergo Mbeya, Christophe Forgez, Guy Friedrich, Nicolas Damay, Khadija EL Kadri Benkara.

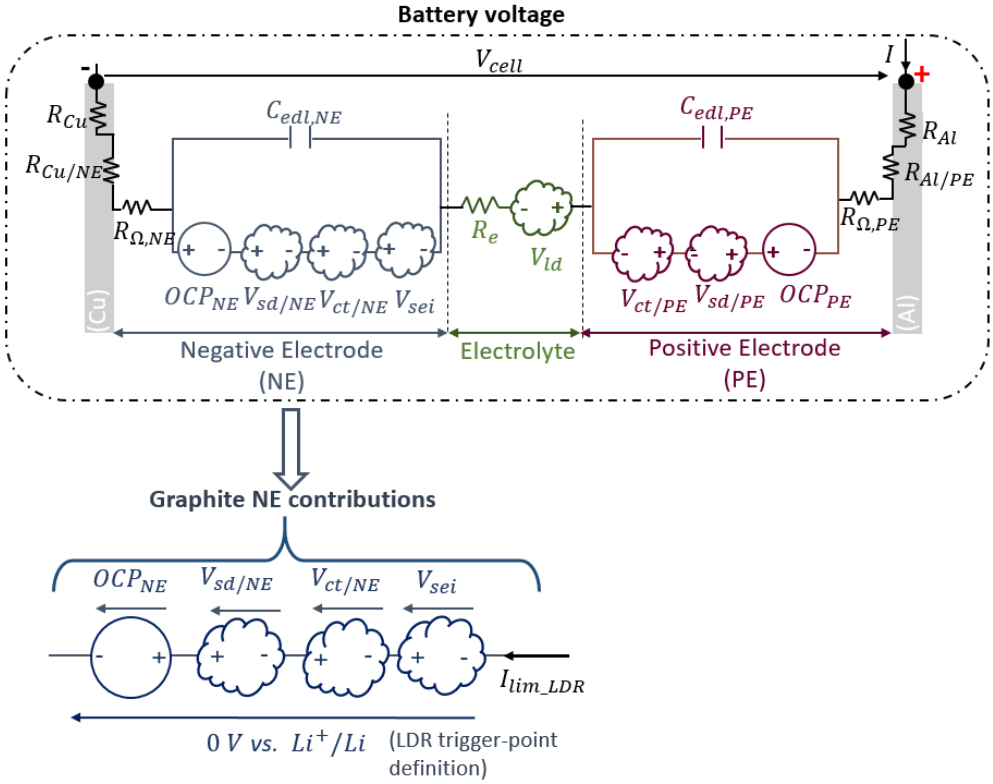

Highlights

Prevention of lithium deposition reaction in Li-ion batteries using a non-invasive approach - Part I : Separation of the negative electrode contributions.

Karrick Mergo Mbeya, Christophe Forgez, Guy Friedrich, Nicolas Damay, Khadija EL Kadri Benkara.

Prevention of lithium deposition reaction in Li-ion batteries using a non-invasive approach - Part I : Separation of the negative electrode contributions.

Karrick Mergo Mbeya, Christophe Forgez, Guy Friedrich, Nicolas Damay, Khadija EL Kadri Benkara.

Sorbonne Université, Université de Technologie de Compiègne, CNRS, FRE 2012 Roberval, Centre de recherche Royallieu, CS 60319, 60203 Compiègne Cedex, France.

Abstract

Many Li-ion cell ageing mechanisms take place at the electrodes. Among these mechanisms, there is the deposit of lithium at the graphite electrode in fast charging conditions of LIBs. This mechanism can be avoided by having a control on the potential of the graphite electrode. This is difficult to achieve because this potential is mixed to others contributions in the battery voltage. In the present paper, we propose a method to separate the potential of the graphite electrode to the battery voltage using a model and characterization of the battery that is non-invasive and easy to implement. The method has been applied to a $LiFePO_4$/graphite battery. The contributions of the SEI, the charge transfer and diffusion of the graphite electrode have been estimated in the battery voltage. The proposed method can be adapted to other Li-ion batteries or other battery technologies using carbon as negative active-material (e.g. sodium ion batteries).

Keywords: Battery, graphite electrode, electrode potential, modeling, lithium plating, ultra-fast charging, non-invasive characterization.

Nomenclature

β_1 Coefficient representing the contributions of the SEI and the NE charge transfer to the battery surface overvoltage.

β_2 Coefficient representing the contributions of the SEI and the NE charge transfer to the battery diffusion overvoltage.

ΔV_{mes} Battery overvoltage measured : difference between V_{cell} and OCV $[V]$

τ_d Time constant of diffusion of battery $[s]$

τ_{surf} Time constant that characterizes the fast dynamic of battery $[s]$

$C_{edl/PE}/C_{edl/NE}$ Electric double layer capacitance of the PE/NE $[F]$

C_{surf} Electric double layer capacitance of battery $[F]$

C_{th} Heat capacity of battery $[J/K]$

I Current of battery [A or C-$rates$]

I_0 Exchange current of the battery $[A]$

I_{lim_LDR} Limit current to prevent the lithium deposition reaction [A or C-$rates$]

OCP_{PE}/OCP_{NE} Equilibrium potentials of the PE/NE vs. reference electrode $[V]$

OCV Equilibrium voltage of battery $[V]$

Q Charge quantity of battery $[Ah]$.

$R_{\Omega,PE}/R_{\Omega,NE}$ Resistance due to the electronic conduction through the solid phases to the PE/NE $[\Omega]$

$R_{Al/PE}/R_{Cu/NE}$ Resistance due to the contacts between the positive/negative active material and current collector $[\Omega]$

R_d Resistance of diffusion of battery $[\Omega]$

R_e Resistance due to the ionic conduction in electrolyte phase $[\Omega]$

R_s Pure ohmic resistance of battery $[\Omega]$

V_{cell} Voltage of a LIB $[V]$

$V_{ct/PE}/V_{ct/NE}$ Overpotential due to the charge transfer at the PE/NE $[V]$

V_d Battery overvoltage caused by the diffusion phenomena $[V]$

V_{ld} Overvoltage due to the diffusion in electrolyte phase $[V]$

$V_{sd/PE}/V_{sd/NE}$	Overpotential due to the diffusion in solid phase at the PE/NE $[V]$
V_{sei}	Overpotential due to the ionic migration through the SEI $[V]$
V_{surf}	Battery overvoltage caused by the internal interface phenomena $[V]$
Z_d	Impedance of diffusion of battery $[\Omega]$
$\partial OCV/\partial T$	Entropy coefficient $[V/K]$
F	Faraday's constant [96485 $C.mol^{-1}$]
R	Gas constant [8.3145 $J.mol^{-1}.K^{-1}$]
DVA	Differential Voltage Analysis
ECM	Equivalent Circuit Model
EIS	Electrochemical Impedance Spectroscopy
GITT	Galvanostatic Intermittent Titration Technique
LDR	Lithium Deposition Reaction
LIB	Lithium Ion Battery
LLI	Lithium Lithium Iventory or lost of lithium
NE	Negative Electrode
PE	Positive Electrode
SEI	Solid Electrolyte Interface
SoC	State of Charge [%]

1. Introduction

The challenge of the optimal fast charging of Li-ion batteries relies on the determination of the current allowing to inject the possible energy maximum into the battery, in a reduced time and without compromised its safety and lifespan.

LIBs have operating limitations, especially when charging at low temperatures or at high current rates. In these conditions, the occurence of the LDR (Lithium Deposition Reaction), the so-called lithium plating, on the graphite NE is well known as one of the main limitations [1, 2, 3]. This unwanted reaction occurs when the interface potential of the graphite NE gets less than 0 V vs. Li^+/Li. It accelerates the performance fading of batteries (capacity loss and impedance increase) and can even cause safety issues by an internal short-circuit between the PE and NE or a thermal runaway of the battery in the worst case [1, 3]. In this point of view, the monitoring of the graphite NE is required to prevent this unwanted reaction and to achieve fast charging in optimal and more safe conditions.

The potential of the graphite NE in a LIB can be obtained by modeling. Electrochemical models allow to achieve that accurately in local scale. Ecker *et al.* [4] described the state-of-the-art in parameterisation. These models require invasive, expensive and time-consuming tests to parameterize. As alternative, physical ECMs separating the contributions of the PE and the NE at macroscopic scale can be used [5, 6]. Merla *et al.* [6] employed a two-electrode ECM with non-invasive and low-cost parametrisation requirements allows quicky and easy tests.

In the present study, we develop a non-invasive approach to separate the macroscopic potential of the graphite electrode in the LIBs. In principle, our approach relies on a simplification of a two-electrode ECM. From the latter, we develop a simplified and non-invasive method to characterize the battery and to separate the contributions of the graphite NE to the battery voltage. The present study is carried out to cylindrical (22650) 2.3 Ah cells consisting of the $LiFePO_4$ PE and the graphite NE.

The remainder of this article is presented as follows. First, we define the LDR trigger-point and we describe a complete two-electrode model of the battery. Second, we introduce the simplification the two-electrode model allowing an easy determination of the parameters from GITT and EIS tests on the battery. Finally, we describe the methodology to separate the contributions of the graphite electrode in the battery voltage.

2. Definition of the LDR trigger-point with a two-electrodes equivalent circuit model

The terminal voltage of a LIB during charge represents various contributions going from the positive terminal to the negative terminal. These contributions are shown in Figure 1a.

Among the aforementioned contributions, only a few are preponderant with respect to the triggering of the LDR in the LIBS. These contributions are : (i) the equilibrium potential of the graphite electrode, (ii) the SEI, (iii) the charge transfer and (iv) the diffusion in solid phase of the graphite NE. Indeed, the OCP of the graphite NE is close to the equilibrium potential of the lithium metal, which intrinsically let a small margin to this electrode regarding the triggering of the LDR. Consequently, if during a charge of a LIB significant limitations of the (i) Li transport in the SEI, (ii) the charge transfer and (ii) the diffusion of the solid phase occur at this electrode, the lithium will be accumulated on surface and the interface potential of the graphite will be driven quickly beyond the trigger-point of the LDR.

The limit point beyond which the LDR is triggered in a LIB corresponds to the moment when the interface potential of the graphite electrode near the separator reaches 0 V vs Li^+/Li. A macroscopic model of the graphite electrode is proposed in order to get this limit point (Figure 1b). As it is shown in Figure 1b, the sum of the overpotentials V_{sei}, $V_{ct,NE}$, and $V_{sd,NE}$ cancels the OCP_{NE} at this point. In adittion, the current flowing through the battery at this point represents the limiting charging current to prevent the LDR (I_{lim_LDR}).

In order to separate the contributions of the graphite electrode giving the limit point of triggering of the LDR, a simplification of the two-electrode ECM of Fig. 1a is introduced in the next section.

3. One-electrode ECM for the experimental characterization

3.1. From the two-electrodes ECM to a one-electrode ECM

The dynamics of the main processes inside the LIBs can be (i) instantaneous, (ii) fast (with time constant from a few microseconds to a few seconds) or (ii) slow (with time constant from a few seconds to a few hours) [7, 8, 9]. Figure 1a shows the grouping of the processes according their dynamics with the Nyquist plot of a LIB impedance (frequency domain). As a consequence, the two-electrode ECM (Fig 1a) is simplified to a one-electrode ECM in figure 2b, where :

- OCV is the difference between OCP_{PE} and OCP_{NE} ;
- R_s represents the sum of the different resistive contributions inside a LIB ;
- V_{surf} is the sum of the contributions of the SEI and the charge transfers of the PE and the NE ;
- the capacitance C_{surf} includes the double layers of the PE and the NE as well as the capacitive effect of the SEI layer [10, 11] ;
- V_d represents the sum of the contributions of the electrolyte phase diffusion and solid phase diffusions at the PE and the NE.

3.1.1. Modeling of the surface and diffusion overvoltages

The expression of V_{surf} is partially inspired from Butler-Volmer law (Eq. (1)) [12]. I_0 is the exchange current of the battery and τ_{surf} is the time constant that characterizes the fast dynamic of the battery.

$$\frac{dV_{surf}}{dt} = \frac{I}{C_{surf}} - \frac{1}{\tau_{surf}} \times \frac{2RT}{F} sinh^{-1}\left(\frac{I}{2I_0}\right), \quad (1)$$

The overall diffusive behavior of the battery is assumed to be Nernst-type diffusion, which the impedance is given by the following equation in the Laplace domain [13] :

$$Z_d(s) = R_d \frac{tanh(\sqrt{\tau_d s})}{\sqrt{\tau_d s}}, \quad (2)$$

with R_d the diffusion resistance of the battery and τ_d the corresponding time constant. The latter characterizes the slow dynamics of the aforementionned processes [7, 8]. By first applying the Mittaf-Lefler theorem and then proceeding by simplifications, the equation (2) can be approximated by an finite series decomposition of parallel RC circuits, which gives the equation (3) [13, 14].

$$Z_d(s) \approx \sum_{k=1}^{N} \frac{R_{d,k}}{1 + \tau_{d,k} s} \quad (3)$$

$R_{d,k}$ and $\tau_{d,k}$ are respectively related to R_d and τ_d by the respective relationships below [15] :

$$R_{d,k} = \frac{8R_d}{\pi^2(2k-1)^2} \quad \text{and} \quad \tau_{d,k} = \frac{4\tau_d}{\pi^2(2k-1)^2}. \quad (4)$$

3.1.2. Temperature, SoC and Current dependences

The parameters R_s, I_0, τ_{surf}, τ_d, and R_d are assumed to be temperature dependent only. In particular, the consequences of neglecting the SoC dependence is likely to lead to inaccuracies at extreme SoC. As a consequence, the model results at SoC less than 10% and more than 90% are treated with great caution. The temperature dependence for each parameter is calculated as follows :

$$\psi(T) = \psi(25^\circ C)\theta_\psi(T), \quad (5)$$

where θ_ψ is a temperature dependence coefficient. At 25 °C, θ_ψ is equal to 1.

3.2. Parameters determination by EIS and GITT

3.2.1. Experimental conditions

The aforementioned parameters have been extracted from GITT and EIS measurements. A Bio-Logic test system (VSP-300), with 0.1% of its full scale, was used to perfom these measurements. The cylindrical commercial $LiFePO_4$/graphite cell (2.3 Ah) was put into a climatic chamber to control its equilibrium temperature.

GITT tests have been performed at 0 °C, 15°C and 25 °C for the following charging currents : 2 A (0.9C),

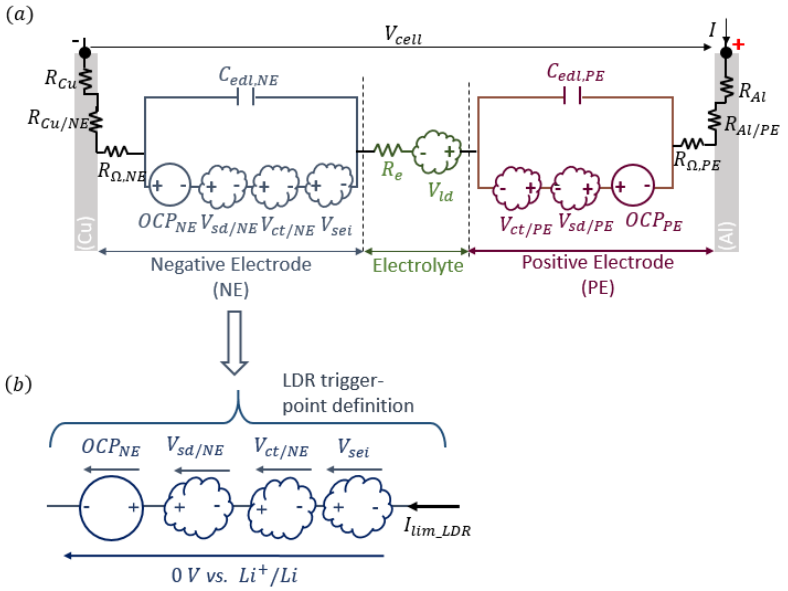

FIGURE 1: (a) Two-electrodes ECM describing the main processes inside a LIB. (b) Definition of LDR trigger-point limit.

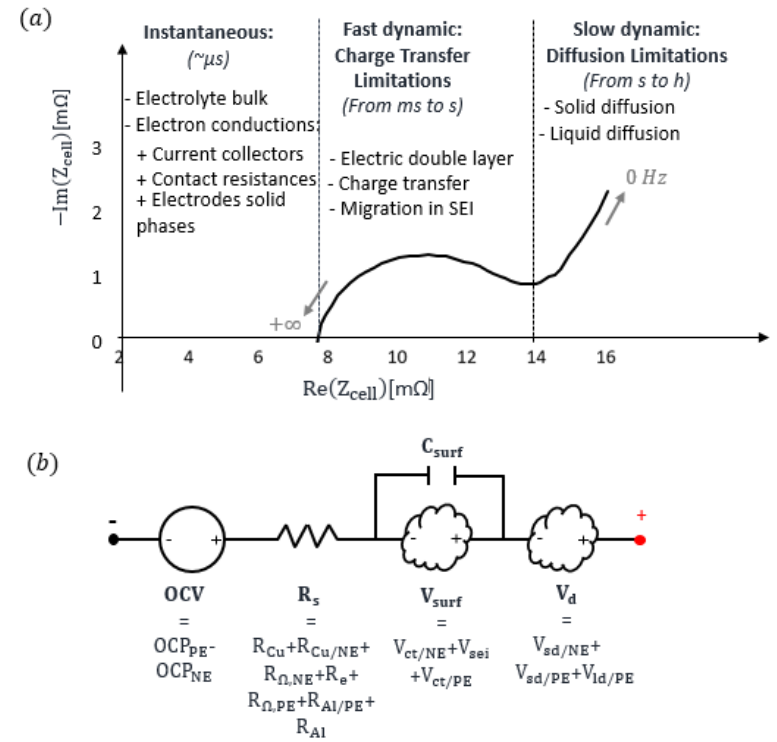

FIGURE 2: (a) Representation of the main processes inside a LIB from its impedance spectrum [7, 9]. (b) One-electrode ECM

6 A (2.6C), 10 A (4.3C), 15 A (6.5C) and 20 A (8.7C). Since the SoC dependence is neglected, each pulse current was applied from 35% and 51%.
EIS tests have been performed at SoC 35%, with a current of amplitude C/10, in the frequency range of 10 kHz-100 mHz and for the following temperatures : 0 °C, 15 °C and 25 °C.

3.2.2. Extraction of parameters by combining different operating points

The resistance R_s was extracted from EIS measurements. As shown in figure 3a, R_s was obtained from the point of intersection of the real axis and the impedance curve (i.e. for $Im(Z_{cell}) = 0$) [6, 12]. Arrhenius' law was then fitted with the obtained values to get the temperature dependence coefficient.

The parameters I_0, τ_{surf}, τ_d and R_d were extracted from GITT measurements. During GITT pulses, the battery temperature varies. As a consequence, the parameters *a priori* evolve with the cell temperature. To take these evolutions into account, we first used the simplified thermal model of Eq. (6) to estimate the cell temperature [16, 15]. Second, as shown in figure 3b, we fitted the model with all GITT measurements simultaneously (i) by using the estimated temperature as one of input data and (ii) by computing the evolving of the parameters with the temperature accoring Eq. (5). Arrhenius' law was used for the temperature coefficient of I_0. τ_{surf}, τ_d and R_d, were considered linear by piece according to the temperature. The parameters obtained are reported in Table 1.

$$C_{th}\frac{dT_{cell}}{dt} = I\Delta V_{mes} + IdT_{cell}\frac{\partial OCV}{\partial T} \tag{6}$$

TABLE 1: Values of parameters R_s, I_0, τ_{surf}, τ_d and R_d extracted from GITT dataset

Parameters		Values		
R_s	$R_s(25°C)\,[m\Omega]$	6,14		
	$E_{a,R_s}\,[kJ/mol]$	2.5		
I_0	$I_0(25°C)\,[A]$	5.5		
	$E_{a,I_0}\,[kJ/mol]$	64.63		
		0 °C	**17 °C**	**25 °C**
$R_d\,[m\Omega]$		26.7	15.8	12.3
$\tau_{surf}\,[ms]$		5.2	3.6	1.2
$\tau_d\,[s]$		41.5	35.7	3.8

4. Separation of the graphite NE contributions in the reduced ECM parameters

4.1. Separation of the equilibrium potentials

In a previous study [17], we proposed a non-invasive method to separate the OCP of the PE and NE in a LIB. The principle of the latter consists in using an optimization algorithm combining the voltage curve of the battery under low current in charge and discharge with the OCPs of half-cells of the PE and NE. Therefore, the OCP of the NE graphite electrode of the studied cell has been obtained in this study.

4.2. Separation of the charge transfer and SEI in the battery overvoltage

Since V_{surf} is resulting from the contribution of the PE, the NE and SEI, the contribution of the graphite NE can be expressed as follows :

$$\begin{aligned} V_{ct,NE} + V_{sei} + V_{ct,PE} &= V_{surf} \\ V_{ct,NE} + V_{sei} &= (1 - \frac{V_{ct,PE}}{V_{surf}})V_{surf} \\ V_{ct,NE} + V_{sei} &= \beta_1 V_{surf}, \end{aligned} \tag{7}$$

where $\beta_1 = 1 - \frac{V_{ct,PE}}{V_{surf}}$. β_1 represents the contributions of the SEI and the charge transfer of the graphite NE in the overall charge transfer of the battery. The value of the latter belongs to the interval [0 :1]. The approach to estimate β_1 is described in below.

- Estimation of the contribution of the SEI and the charge transfer of the graphite NE

Numerous studies in the literature tend to show that the contributions of SEI and charge transfer of the graphite electrode dominate the overall charge transfer of LIBs [18, 19, 20, 21, 22, 23, 24].

The data from Illig *et al.* study [18] gives that the graphite electrode contributed about 80% in the overall charge transfer of a cell $LiFePO_4$/graphite.

By comparing the behaviors of graphite/Li cells and $LiFePO_4$/Li cells at low temperature, Li *et al.* [19] observed that the contributions of SEI and charge transfer were the limiting factor in the graphite/Li cells, while the ionic conductivity was the limiting factor in the $LiFePO_4$/Li cells [19].

Smart *et al.* [20] observed that before the formation of the SEI, the interfacial resistance of the $LiNi_{0.8}Co_{0.2}O_2$ electrode dominated that of the graphite electrode, while after the SEI formation, the interfacial resistances of both electrodes were equivalent. This demonstrates how the SEI impacts the graphite interface since the $LiNi_{0.8}Co_{0.2}O_2$ electrode is known to have a highly resistive interfacial film [25].

The study of Jones *et al.* [21] on NCA/graphite cells showed that the interface resistance of the graphite electrode was higher compared to that of the NCA electrode, about 3 and 10 times higher at 23 °C and -30 °C respectively [21].

The data from Yang *et al.* study [22] show that the charge transfer (and the SEI) overpotential of the graphite electrode represents almost the overall charge transfer overvoltage of a NMC/graphite cell over the entire range of SoC for new and aged cells (after 3300 cycles).

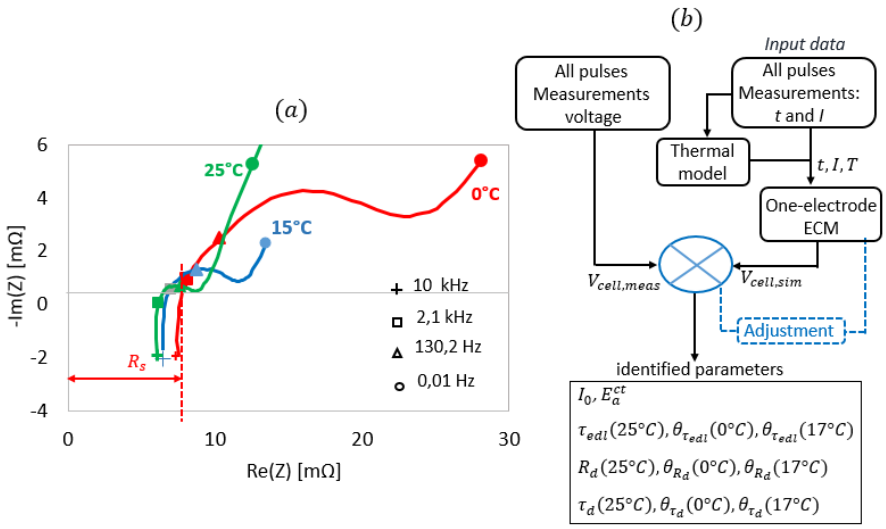

FIGURE 3: (a) EIS measurements at 0 °C, 15 °C, 25 °C and illustration of extraction of R_s at 0 °C. (b) Schematic of the extraction of the parameters I_0, τ_{surf}, τ_d and R_d, using a global adjustment on GITT dataset.

In their recent review on the study of phenomena limiting charge transfer, Jow *et al.* [24] concluded that the charge transfer of LIBs is mainly dominated by the SEI.

The various studies mentioned above suggest that the contributions of the SEI and the graphite NE charge transfer would be predominant in the overall charge transfer of Li-ion batteries at T ≤ 25 °C, which particularly coincides with the conditions where the LDR is more favored [26].

Based on these studies,we therefore made a simplifying hypothesis to get β_1. This considering that the overall charge transfer overvoltage of the cell is essentially the contributions of the SEI and the NE charge transfer, whatever the operating temperature. Consequently β_1 is approximated to 1 (Eq. (8)).

$$\begin{aligned} V_{ct,NE} + V_{sei} &= \beta_1 V_{surf} \\ &\approx V_{surf}, \text{ with } \beta_1 \simeq 1 \end{aligned} \tag{8}$$

4.3. Separation of the solid diffusion contribution to battery overvoltage

By proceeding in the same way as before, we express the diffusion overpotentials of the graphite NE as follows :

$$V_{sd,NE} = \beta_2 V_d, \tag{9}$$

with β_2 the solid diffusion contribution of the graphite NE, which value is defined in the interval [0 :1]. The method to identify the value of β_2 is described in below.

- Estimation of the diffusion contribution of the graphite NE using the trigger limit of LDR of cell

The value of β_2 is determined empirically by searching the trigger limit of the LDR of the battery. Indeed, from the definition LDR trigger-point limit introduced previously (see Fig. 1b), the quantities OCP_{NE}, $V_{ct,NE}$ and V_{sei} are now known, while the current I_{lim_LDR} and the coefficient $V_{sd,NE}$ still remain unknown. As the value of $\beta_{sd,NE}$ should be *a priori* between 0 and 1, this value can be defined as the smallest value includes in [0 :1] that yields the current I_{lim_LDR}. In other words, β_2 allows to determine the charge limit current close to LDR and *vice versa*.

An experimental approach based on the "trial-error" method is proposed to get the value of β_2 in the interval [0 :1] (Figure 4). Since OCP_{NE}, $V_{ct,NE}$ and V_{sei} are now known are known, the following operations can be carried out :

1. β_2 is initially assumed equal to 0 (step 1);
2. a current I_{lim_LDR} is calculated using Eq. (10) (step 2);
3. the precomputed current is applied to the battery in order to evaluate if it leads to the LDR (steps 3 and 4). If the LDR occurs, the present value of β_2 must be incremented by 0.1 before returning to step 2. otherwise, there are two possibilities. The first one is the case where β_2 is equal to 0 or 1. In this case, we would get exactly the required minimum value. The second one corresponds to the case where the value of β_2 is different from 0 or 1. As shown in

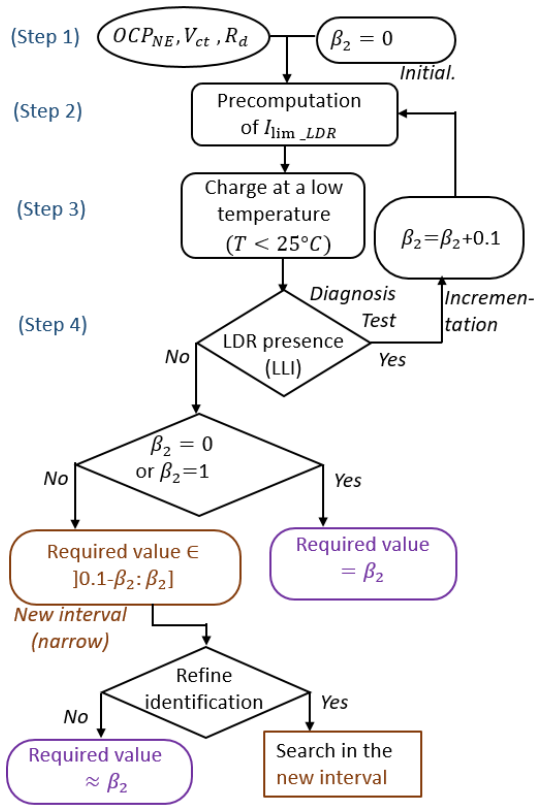

FIGURE 4: Diagram of the method to separate the contribution of solid diffusion of the graphite NE from the resistance of diffusion of the cell.

figure 4, a new interval (very narrow) belonging to the required minimum value is found.

In order to simplify the calculations of the current I_{lim_LDR}, the overvoltages V_{surf} and V_d are taken in steady state. This results in a more optimistic consideration with regard to the occurrence of the LDR over time. In other words, the delay brought by the capacitive effects of the double layer capacitance and the diffusion are neglected. The current I_{lim_LDR} can be calculated from Eq. (10).

$$OCP_{NE}(SoC) - \frac{2RT}{F} sinh^{-1}\left(\frac{I_{lim\_LDR}}{2I_0(T)}\right) - \beta_2 R_d(T) I_{lim\_LDR} = 0 \quad (10)$$

Since the LDR is favored cold, it seems opportune to carry out the tests to get β_2 below 25 °C. In addition, at cold temperatures the ageing mechanisms, such as the growth of SEI [27, 28] or the dissolution of metals in the PE are negligible [29, 26, 30].

The DVA is proposed to detect the LDR. This technique of the battery degradation diagnostic is based on the evolution of the peaks of the curve $dV_{cell}/dQ = f(Q)$ at low current. Many authors in the literature have used this technique to study LDR [31, 32, 33]. Since the deposit lithium can be partially or totally irreversible, its presence after a charge event can be seen as the so-called LLI, which can be detected using DVA. In the present study, if a loss of active material is detected by DVA after a charge event, it would be considered that a mechanical degradation of the electrodes. This because the LDR is likely to cause such degradation in the long term [31, 22].

4.4. *Experiments to identify the solid diffusion contribution of the graphite NE*

The tests to identify β_2 have been carried out on a narrow SoC range (see Fig. 5) in order to work with constant currents. Indeed, as the current I_{lim_LDR} *a priori* varies with the temperature and the SoC, working on such a range of SoC allows to minimize these variations. The current I_{lim_LDR} can be considered constant, which therefore simplifies the experimental implementation. The experimental protocol consisted of charging

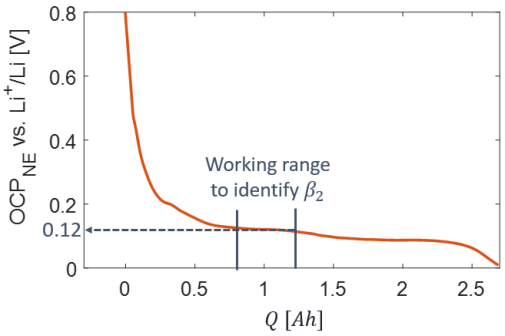

FIGURE 5: Representation of the working range for the identification β_2 on the curve of OCP_{NE}=$f(Q)$.

the cell from initial SoC (35%) to final SoC of the study (51%) with the precomputed current I_{lim_LDR} at 0 °C. A 1 A (0.4C) discharge was also performed to return the cell to the initial SoC. Between charge and discharge, the cell was relaxed for 1 hour. These operations were repeated 22 times in order to allow that a possible presence of the LDR to be detectable and quantifiable.

These tests have been performed at 0 °C since it is widely reported that the LDR is the predominant degradation mechanism that can induce the LLI at a such temperature [26, 32, 33]. Two precomputed currents, 6.5 A~3 C and 5 A~2 C, have been tested. These currents correspond respectively to $\beta_2 = 0$ and $\beta_2 = 0.1$. We were limited to 0.1, because we found that by working with $\beta_2 = 0$, the corresponding current led to the LDR, while

with $\beta_2 = 0.1$, the corresponding current did not cause the LDR. The results obtained with both values of β_2 are discussed in detail in paragraph 4.5.

Before and after the application of this protocol, the cell was charged and discharged at 0 °C with a current of C/25 in order to assess the presence of the LDR. As mentioned previously, the DVA technique is used to identify the presence of the LDR through the LLI [31, 32, 33].

4.5. Results and dicussion

4.5.1. Working with β_2 equal to 0

By working with β_2 equal to 0, it is implicitly supposed that there is no limitation of the solid diffusion of the graphite NE. The solid diffusion of the cell is that of the $LiFePO_4$ PE. In this configuration, the LDR has been detected.

Figure 6a shows the profiles of the differential voltage obtained before and after working with β_2 equal to 0. As the measurements were performed at 0 °C, only the transition between plateaus P_3 and P_2 is clearly visible on the voltage profile at C/25 (Fig. 6b). As a consequence, this transition corresponds to the unique peak that is observed on both profiles of the differential voltage (Fig. 6a).

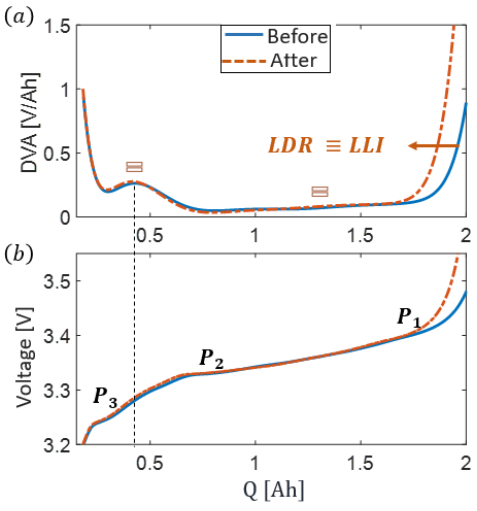

FIGURE 6: (a) Profiles of the differential voltage obtained before and after charge by working with β_2 equal to 0 and (b) the corresponding voltage profiles (at C/25 and 0 °C).

By comparing the two profiles of differential voltage, one can be noticed that (i) the rise of the curve towards the high Q, (> 1.5 Ah), occurs earlier with the profile obtained after the charge test and (ii) the two profiles are identical over the remaining SoC range (≤ 1.5 Ah). It means that there was a loss of lithium inventory caused by LDR by working with β_2 equal to 0. The amount of the lithium deposit was estimated at about 4% of the loss of the battery capacity.

4.5.2. Working with β_2 equal to 0.1

By working with β_2 equal to 0.1, it is supposed that the contribution of the solid diffusion of the graphite electrode represents 10% of the overall diffusion of the cell. In this configuration, there was no LDR.

Figure 7 shows the profiles of the differential voltage obtained before and after working with β_2 equal to 0.1. It can be noticed that both profiles are identical, which means that there was no LDR during the charge tests by working with β_2 equal to 0.1. In other words, for the studied cell, the value of β_2 should be sought in a narrow interval (]0 :0.1]) instead of a large interval defined initially ([0 :1]).

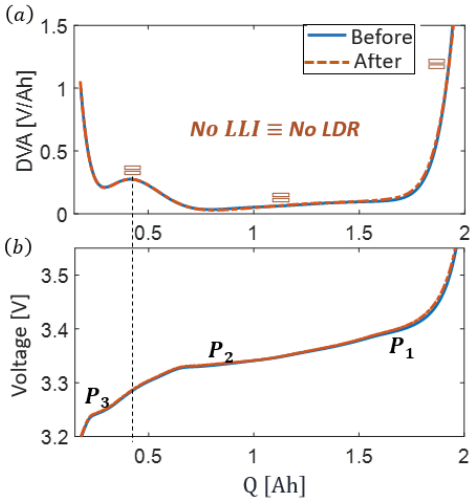

FIGURE 7: (a) Profiles of the differential voltage obtained before and after charge by working with β_2 equal to 0.1 and (b) the corresponding voltage profiles (at C/25 and 0 °C).

We have thus chosen to estimate the contribution of solid diffusion of the graphite electrode by considering β_2 equal to 0.1 (Eq. (11)).

The low contribution of the graphite electrode in the overall diffusion resistance reflects the results obtained by Illig *et al.* [18] on a $LiFePO_4$/graphite cell, where the solid diffusion contribution of graphite was lower than that of the $LiFePO_4$. In addition, it is reported that the limitation of solid diffusion is inherently very marked in the $LiFePO_4$ due to its 1D dimension structure [34, 35]. It may be possible that the diffusion contribution of the $LiFePO_4$ electrode dominates the overall diffusion

of the studied cell.

$$\begin{aligned} R_2(T) &= \beta_2 \times R_d(T) \\ &\simeq 0,1 \times R_d(T) \end{aligned} \tag{11}$$

5. Conclusion and next work

A non-invasive separation of the graphite electrode potential in the LIBs has been established. First, a electric model of the battery taking temperature into account has been developed. The parameters of the latter have been determined using an accurate method coupling EIS and GITT measurements of the battery. This model has been evolved to the level of electrodes in order to separate the contribution of the graphite NE, which includes its overpotentials caused by the SEI layer and the phenomena of the charge transfer and the diffusion.

Based on literature studies, it was noticed that the SEI and the charge transfer at the graphite electrode tends to dominate the charge transfer limitations in LIBs. Thus, we assumed that the overall charge transfer of the battery was mostly the contributions of the SEI and the charge transfer of the graphite electrode. Moreover, the contribution of the diffusion of the graphite NE has been determined empirically. It has been estimated that the diffusion of the graphite NE contributes to 10% in the overall diffusion of the battery.

In principle, the proposed method is not specific to LiFePO4/graphite batteries. It should be applicable to other battery electrodes having similar electrochemical characteristics and mechanisms. The second part of this work focuses on the estimation of limit current of the cell and its experimental examination on the cell performance.

Acknowledgements

We thank the ministry of national education of France and the region of Hauts-de-France for granting this PhD research work.

Références

[1] Z. Li, J. Huang, B. Y. Liaw, V. Metzler, J. Zhang, A review of lithium deposition in lithium-ion and lithium metal secondary batteries, Journal of Power Sources 254 (2014) 168–182. doi :10.1016/j.jpowsour.2013.12.099.

[2] T. Waldmann, B.-I. Hogg, M. Wohlfahrt-Mehrens, Li plating as unwanted side reaction in commercial Li-ion cells – A review, Journal of Power Sources 384 (2018) 107–124. doi :10.1016/j.jpowsour.2018.02.063.

[3] A. Tomaszewska, Z. Chu, X. Feng, S. O'Kane, X. Liu, J. Chen, C. Ji, E. Endler, R. Li, L. Liu, Y. Li, S. Zheng, S. Vetterlein, M. Gao, J. Du, M. Parkes, M. Ouyang, M. Marinescu, G. Offer, B. Wu, Lithium-ion battery fast charging : A review, eTransportation 1 (2019) 100011.

[4] M. Ecker, T. Tran, P. Dechent, S. Käbitz, A. Warnecke, D. Sauer, Parameterization of a physico-chemical model of a lithium-ion battery : I. determination of parameters, Journal of the Electrochemical Society 162 (2015) A1836–A1848. doi :10.1149/2.0551509jes.

[5] R. Scipioni, P. S. Jørgensen, C. Graves, J. Hjelm, S. Jensen, A Physically-Based Equivalent Circuit Model for the Impedance of a LiFePO ₄ /Graphite 26650 Cylindrical Cell, Journal of The Electrochemical Society 164 (9) (2017) A2017–A2030. doi :10.1149/2.1071709jes.
URL http://jes.ecsdl.org/lookup/doi/10.1149/2.1071709jes

[6] Y. Merla, B. Wu, V. Yufit, R. Martinez-Botas, G. Offer, An easy-to-parameterise physics-informed battery model and its application towards lithium-ion battery cell design, diagnosis, and degradation, Journal of Power Sources 384 (2018) 66–79. doi :10.1016/j.jpowsour.2018.02.065.

[7] A. Jossen, Fundamentals of battery dynamics, Journal of Power Sources 154 (2) (2006) 530 – 538, selected papers from the Ninth Ulm Electrochemical Days. doi :https ://doi.org/10.1016/j.jpowsour.2005.10.041.

[8] J. Huang, Z. Li, J. Zhang, S. Song, Z. Lou, N. Wu, An analytical three-scale impedance model for porous electrode with agglomerates in lithium-ion batteries, Journal of the Electrochemical Society 162 (2015) A585–A595. doi :10.1149/2.0241504jes.

[9] U. Krewer, F. Röder, E. Harinath, R. Braatz, B. Bedürftig, R. Findeisen, Review—dynamic models of li-ion batteries for diagnosis and operation : A review and perspective, Journal of The Electrochemical Society 165 (2018) A3656–A3673. doi :10.1149/2.1061814jes.

[10] P. Balbuena, Y. Wang, Lithium-Ion Batteries, Solid-Electrolyte Interphase, Imperial College Press, 57 Shelton Street Covent Garden London WC2H 9HE, 2004. doi :10.1142/p291.

[11] T. Kranz, S. Kranz, A. Jaegermann, B. Roling, Is the solid electrolyte interphase in lithium-ion batteries really a solid electrolyte ? transport experiments on lithium bis(oxalato)borate-based model interphases, Journal of Power Sources 418 (2019) 138–146. doi :10.1016/j.jpowsour.2019.01.060.

[12] L. Juang, P. Kollmeyer, T. Jahns, R. Lorenz, Improved modeling of lithium-based batteries using temperature-dependent resistance and overpotential, in : Conference : 2014 IEEE Transportation Electrification Conference and Expo (ITEC), 2014, pp. 1–8. doi :10.1109/ITEC.2014.6861800.

[13] E. Kuhn, C. Forgez, P. Lagonotte, G. Friedrich, Modelling ni-mh battery using cauer and foster structures, Journal of Power Sources 158 (2006) 1490–1497.

[14] N. Damay, C. Forgez, G. Friedrich, M.-P. Bichat, Heterogeneous behavior modeling of a $LiFePO_4$-graphite cell using an equivalent electrical circuit, Journal of Energy Storage 12 (2017) 167–177. doi :10.1016/j.est.2017.04.014.

[15] N. Damay, C. Forgez, M.-P. Bichat, G. Friedrich, Thermal modeling of large prismatic lifepo4-graphite battery. coupled thermal and heat generation models for characterization and simulation, Journal of Power Sources 283 (2015) 37–45. doi :10.1016/j.jpowsour.2015.02.091.

[16] C. Forgez, D. Vinh Do, G. Friedrich, M. Morcrette, C. Delacourt, Thermal modeling of a cylindrical LiFePO4/graphite lithium-ion battery, Journal of Power Sources 195 (9) (2010) 2961–2968. doi :10.1016/j.jpowsour.2009.10.105.

[17] K. M. Mergo, N. Damay, G. Friedrich, C. F., M. J., Offline method to determine the electrode balancing of li-ion batteries, Mathematics and Computers in Simulation (2020). doi :https ://doi.org/10.1016/j.matcom.2020.02.013.

[18] J. Illig, J. P. Schmidt, M. Weiss, A. Weber, E. Ivers-Tiffée, Understanding the impedance spectrum of 18650 $LiFePO_4$-cells, Journal of Power Sources 239 (2013) 670–679.

doi :10.1016/j.jpowsour.2012.12.020.

[19] J. Li, C. Yuan, Z. Guo, Z. Zhang, Y. Lai, J. Liu, Limiting factors for low-temperature performance of electrolytes in lifepo4/li and graphite/li half cells, Electrochimica Acta 59 (2012) 69–74. doi :10.1016/j.electacta.2011.10.041.

[20] M. Smart, B. Lucht, S. Dalavi, F. Krause, B. Ratnakumar, The effect of additives upon the performance of mcmb/lini$_x$co$_{1-x}$o$_2$ li-ion cells containing methyl butyrate-based wide operating temperature range electrolytes, Journal of The Electrochemical Society 159 (2012) A739. doi :10.1149/2.058206jes.

[21] J.-P. Jones, M. Smart, F. Krause, B. Ratnakumar, E. Brandon, The effect of electrolyte composition on lithium plating during low temperature charging of li-ion cells, ECS Transactions 75 (2017) 1–11. doi :10.1149/07521.0001ecst.

[22] X.-G. Yang, Y. Leng, G. Zhang, S. Ge, C.-Y. Wang, Modeling of lithium plating induced aging of lithium-ion batteries : Transition from linear to nonlinear aging, Journal of Power Sources 360 (2017) 28 – 40. doi :https ://doi.org/10.1016/j.jpowsour.2017.05.110.

[23] R. Jow, M. Marx, J. Allen, Distinguishing li^+ charge transfer kinetics at nca/electrolyte and *Graphite*|*Electrolyte* interfaces, and *NCA*|*Electrolyte* and *LFP*|*Electrolyte* interfaces in li-ion cells, Journal of The Electrochemical Society 159 (2012) A604. doi :10.1149/2.079205jes.

[24] R. Jow, S. Delp, J. Allen, J.-P. Jones, M. Smart, Factors limiting li^+ charge transfer kinetics in li-ion batteries, Journal of The Electrochemical Society 165 (2018) A361–A367. doi :10.1149/2.1221802jes.

[25] J. Vetter, P. Novák, M. R. Wagner, C. Veit, K. C. Möller, J. O. Besenhard, M. , M. Wohlfahrt-Mehrens, C. Vogler, A. Hammouche, Ageing mechanisms in lithium-ion batteries, Journal of Power Sources 147 (1-2) (2005) 269–281. doi :10.1016/j.jpowsour.2005.01.006.

[26] T. Waldmann, M. Wilka, M. Kasper, M. Fleischhammer, M. Wohlfahrt-Mehrens, Temperature dependent ageing mechanisms in Lithium-ion batteries - A Post-Mortem study, Journal of Power Sources 262 (2014) 129–135. doi :10.1016/j.jpowsour.2014.03.112.

[27] M. Broussely, S. Herreyre, P. Biensan, P. Kasztejna, K. Nechev, R. Staniewicz, Aging mechanism in li ion cells and calendar life predictions, Journal of Power Sources 97-98 (2001) 13–21.

[28] M. Broussely, P. Biensan, F. Bonhomme, P. Blanchard, S. Herreyre, K. Nechev, J. R. Staniewicz, Main aging mechanisms in li ion batteries, Journal of Power Sources 146 (2005) 90–96.

[29] M. Koltypin, D. Aurbach, L. Nazar, B. Ellis, On the stability of lifepo olivine cathodes under various conditions (electrolyte solutions, temperatures) 10 (2007) A40–A44.

[30] D. Li, Aging mechanisms of li-ion batteries : seen from an experimental and simulation point of view, Ph.D. thesis, Department of Chemical Engineering and Chemistry, page 114 (2017).

[31] N. Legrand, B. Knosp, P. Desprez, F. Lapicque, S. Raël, Physical characterization of the charging process of a Li-ion battery and prediction of Li plating by electrochemical modelling, Journal of Power Sources 245 (2014) 208–216. doi :10.1016/j.jpowsour.2013.06.130.

[32] M. Petzl, M. Kasper, M. A. Danzer, Lithium plating in a commercial lithium-ion battery - A low-temperature aging study, Journal of Power Sources 275 (2015) 799–807. doi :10.1016/j.jpowsour.2014.11.065.

[33] M. Ecker, P. Shafiei S., D. U. Sauer, Influence of operational condition on lithium plating for commercial lithium-ion batteries – Electrochemical experiments and post-mortem-analysis, Applied Energy 206 (2017) 934–946. doi :10.1016/j.apenergy.2017.08.034.

[34] M. Park, X. Zhang, M. Chung, G. B. Less, A. Sastry, A review of conduction phenomena in li-ion batteries, Journal of Power Sources 195 (24) (2010) 7904 – 7929. doi :https ://doi.org/10.1016/j.jpowsour.2010.06.060.

[35] J. Come, Caractérisation électrochimique de matériaux à insertion de li pour supercondensateurs hybrides à haute densité d'énergie, Ph.D. thesis, Université de Toulouse, p. 86-90 et p.111 (2012).
URL `http://www.theses.fr/2012TOU30258`